Eur Biophys J (1984) 11:61–76

European Biophysics Journal

Investigation of pH-induced symmetry distortions of the prosthetic group in oxyhaemoglobin by resonance Raman scattering

R. Schweitzer-Stenner, W. Dreybrodt, D. Wedekind, and S. el Naggar

Universität Bremen, Fachbereich 1 – Physik, D-2800 Bremen 33, Federal Republic of Germany

Received March 22, 1984/Accepted May 10, 1984

Abstract. The depolarisation ratio and the excitation profiles of some prominent Raman lines of the oxyhaemoglobin spectrum (1,375 cm^{-1}, 1,583 cm^{-1}, 1,638 cm^{-1}) have been measured as functions of the exciting laser frequency. The depolarisation ratio shows a complicated minimum-maximum structure in the preresonant region between Soret- and β-band of the optical spectrum, which depends on the pH-value of the solution. These dispersion curves are interpreted by fifth-order Loudon theory of the polarisability tensor including static distortions of the haem group, which lower its symmetry from the ideal D_{4h}-symmetry, and enhancement by a second, non-Raman-active phonon. The fitting constants needed to fit the experimental data are related to static distortions of A_{1g}, B_{1g}, B_{2g}, and A_{2g} symmetry types and thus give information on the symmetry lowering from D_{4h}. The variation of the fitting constants with the pH-value of the solution is interpreted to be caused by protonation/deprotonation processes of titrable amino acid groups contributing to the alkaline and acid Bohr effect. The protonation changes the electrostatic interaction energies in the globular protein and destabilises the salt bridge between His(HC3)β and Asp(FG1)β in the *R*-state. These processes induce distortions of the haem group via haem-apoprotein interactions. Our results give no indication for a dominant role of the covalent Fe^{2+}-N [His(F8)] bond in this process. They are in agreement, however, with the allosteric model of Hopfield, which assumes all interactions to be evenly distributed all over the protein molecule.

Key words: Oxyhaemoglobin, resonance Raman scattering, dispersion of depolarisation ratio, fifth-order Raman theory, alkaline Bohr effect

List of abbreviations:

DPR:	depolarisation ratio
EP:	excitation profile
oxyHb:	oxyhaemoglobin
deoxyHb:	deoxyhaemoglobin
HbA:	human adult haemoglobin
metMbCN:	metmyoglobincyanide
metHbCN:	methaemoglobincyanide
BME:	*bis*(N-maleimidomethyl)ether

Introduction

Interactions between the functional group and the globular protein of haem proteins have been investigated by resonance Raman scattering (Shelnutt et al. 1979, 1980, 1983; Nagai et al. 1980), NMR studies (Lindstrom and Ho 1973; Nagai et al. 1982; LaMar et al. 1978), absorption spectroscopy (Soni and Kiesow 1977; Alben and Bare 1978) and EXAFS experiments (Eisenberger et al. 1976, 1978; Shulman et al. 1982). However, a unique theory of such interactions which is related to ligation and protonation processes (Bohr effect) has not yet been given.

A suitable tool to detect the influence of the globular protein on the haem chromophore is the measurement and analysis of the depolarisation ratio (DPR) dispersion and the excitation profiles (EPs) of Raman lines. Shelnutt (1980) and Zgierski and Pawlikowski (1982) have calculated theoretical DPR and EPs curves of metalloporphyrins, including contributions from electronic and vibrational distortion into the polarisability tensor. Schweitzer et al. (1982) have shown that the DPR dispersion of prominent oxyhaemoglobin – Raman lines varies with the pH-value of the solution, especially in the physiological region. This has been interpreted (Schweitzer-Stenner et al. 1984) as being caused by haem-apoprotein interactions, triggered by protonation/deprotonation of titrable groups. From the fact that haem proteins such as deoxyMb, MbCN and HbCN (Antonini and Brunori 1971), which do not show

any Bohr effect, also do not show any variation of DPR and EPs with changing pH-value of the solution, we may conclude that the groups which trigger the changes in deoxyHb and oxyHb are those which are also related to the Bohr effect in these materials. In the following we will show that there is experimental evidence to support this assumption.

By fitting the pH-dependent DPR-dispersion curves and the corresponding EPs of the 1,355 cm^{-1}, 1,584 cm^{-1}, and 1,638 cm^{-1} Raman lines between pH = 5.5 and 9.5 to a theoretically derived expression, obtained from the formalism of Loudon (1973) in the fifth order, we have interpreted the pH-dependence of the haem-apoprotein interaction. From this we obtain fitting parameters $C_{es}^{\Gamma_{Rj}}\, C_{es}^{\Gamma_j}$, which are related linearly to static A_{1g}, B_{1g}, B_{2g}, A_{2g}, distortions of the haem groups from its ideal D_{4h}-symmetry.

The results of the fitting procedure enable us to correlate protonation/deprotonation processes of Bohr groups with symmetry distortions of the haem group. The corresponding haem-apoprotein interactions are discussed in the light of the allosteric model of Hopfield (1973).

Theoretical background

As we have shown in a previous paper (Schweitzer-Stenner et al. 1984), the polarisability tensor of the oxidation marker line at 1,355 cm^{-1} of the deoxyhaemoglobin spectrum can be written in terms of Loudon's theory (Loudon 1973; Peticolas et al. 1970).

$$\beta_{\varrho\sigma} = \sum_{e,s=Q,B} \left[\frac{M_\varrho^{ge} M_\sigma^{sg} (H_{es}^R + \sum_j H_{es}^{Rj})}{(\tilde{\nu}_e + \Omega_R - \tilde{\nu}_L + i\gamma^e)(\tilde{\nu}_S - \tilde{\nu}_L + i\gamma^s)} + \frac{M_\sigma^{ge} M_\varrho^{sg} (H_{es}^R + \sum_j H_{es}^{Rj})}{(\tilde{\nu}_e - \Omega_R + \tilde{\nu}_L + i\gamma^e)(\tilde{\nu}_S + \tilde{\nu}_L + i\gamma^s)} \right] \quad (1)$$

e, s are frequency indices for the electronic transitions at wave numbers $\tilde{\nu}_Q$ and $\tilde{\nu}_B$ related to the α-band (Q) and Soret-band (B), $\tilde{\nu}_L$ is the wave number of the incident photon, and Ω_R the wave number of Raman-active molecular vibrations. $M_\varrho^{g,e}$, $M_\sigma^{s,g}$ are dipole matrix elements connecting the ground state $|g\rangle$ and the excited electronic state $|e\rangle$, $|s\rangle$. H_{es}^R is the vibronic coupling matrix element of the Raman-active vibration R, which couples the two exited states $|e\rangle$ and $|s\rangle$. The matrix element

$$H_{es}^{Rj} = \left\langle e \left| \frac{\partial^2 H}{\partial Q^{\Gamma_R}\, \partial Q^{\Gamma_j}} \right| s \right\rangle \delta Q^{\Gamma_j} \quad (2)$$

contains the first term of a Taylor expansion of the vibronic coupling operator $\partial H/\partial Q^{\Gamma_R}$ with respect to symmetry-classified static distortions δQ^{Γ_j}, lowering the ideal D_{4h}-symmetry of the haem group. It transforms according to the product representation $\Gamma_R \times \Gamma_j$ (Γ_R, Γ_j are the representations of the Raman-active vibrations Q_R and the static distortion δQ_j respectively). Since in haemoglobin one obtains the Raman tensor by summing only over two excited states $|Q\rangle$ and $|B\rangle$, which both transform like E_u, the second-order vibronic coupling element only gives contributions to $\beta_{\varrho\sigma}$, if $\Gamma_R \times \Gamma_j$ transforms like $E_u \times E_u = A_{1g} + B_{1g} + B_{2g} + A_{2g}$ in D_{4h}.

Thus, the polarisibility tensor can be written as a linear combination of McClain tensors (McClain 1971) according to D_{4h}-symmetry

$$\hat{\beta} = \alpha_{QB}^{A_{2g}}\, \hat{T}^{A_{2g}} F_{QB}^{\tilde{a}}(\tilde{\nu}_Q, \tilde{\nu}_B) + \sum_{e,s=Q,B} \left\{ \left(\sum_\Gamma \alpha_{es}^\Gamma\, \hat{T}^\Gamma \right) [F_{es}^{s}(\tilde{\nu}_e, \tilde{\nu}_s)] \right. \quad (3)$$

with

$$F_{es}^{\tilde{s},\tilde{a}}(\tilde{\nu}_e, \tilde{\nu}_s) = \frac{1}{(\tilde{\nu}_e + \Omega_R - \tilde{\nu}_L + i\gamma^e)(\tilde{\nu}_s - \tilde{\nu}_L + i\gamma^s)} + \frac{1}{(\tilde{\nu}_e - \Omega_R + \tilde{\nu}_L + i\gamma^e)(\tilde{\nu}_s + \tilde{\nu}_L + i\gamma^s)} \pm \frac{1}{(\tilde{\nu}_e - \tilde{\nu}_L + i\gamma^e)(\tilde{\nu}_s + \Omega_R - \tilde{\nu}_L + i\gamma^s)} \pm \frac{1}{(\tilde{\nu}_e + \tilde{\nu}_L + i\gamma^e)(\tilde{\nu}_s - \Omega_R + \tilde{\nu}_L + i\gamma^s)} \quad (4)$$

α_{es}^Γ are complex constants for each tensor $\hat{T}^\Gamma$ of representation Γ and contain the matrix elements H_{es}^R, $H_{es}^{R,j}$. The α_{es}^Γ are related linearly to symmetry-lowering static distortions δQ^{Γ_j} of the haem group.

Using Eq. (3) one is able to calculate the DPR dispersion curves and the corresponding EPs of the 1,355 cm^{-1} deoxyhaemoglobin Raman line for different pH-values of the solution, using Placzek formalism (1934). This simple model is confirmed by the fact that in the case of deoxymyoglobin and MbCN the set of data, obtained from measurements in crystals and solution, can be related to one common polarisibility tensor (el Naggar et al. 1984).

One problem of this theoretical approach, however, could not be solved. All fitting constants α_{es}^Γ have to be taken as complex parameters, although the electronic wave functions representing the basis for the calculation of the matrix elements α_{es}^Γ of Eq. (1) can be chosen as real. From this we conclude that frequency functions of higher-order terms, which are simulated by complex constants, contribute to the scattering tensor.

Regarding this point, we will extend our theoretical basis to avoid complex transition-matrix elements.

In a previous paper (Schweitzer-Stenner et al. 1984) we have anticipated the fact that the DPR and EPs of three oxyHb Raman lines could not be fitted simultaneously using Eq. (1), because a small resonance enhancement takes place between 20,500 cm^{-1} and 20,000 cm^{-1} excitation wave number. To simulate this, we introduce additional 0−1 resonance terms for the Q- and B-state into the PNSF formalism (Peticolas et al. 1970), weighting them with constants C_{QQ}, C_{BB}, and C_{QB}, which are related to Franck-Condon integrals of Q- and B-states and to vibronic coupling into the Q-state respectively. This corresponds to contributions from the β-band and the vibronic sideband of β-band, which in this approximation is treated as an extra electronic transition and included in the summation. This leads to extra contributions to Eq. (1), which are different from those by energy denominators corresponding to the transitions $|g, 0\rangle \rightarrow |Q, 1\rangle$ and $|g, 0\rangle|g, 0\rangle \rightarrow |B, 1\rangle|B, 1\rangle$ (0,1 labels the occupation number of the μ-th phonon). Now one can formulate the following equation:

$$\hat{\beta} = \alpha_{QB}^{A2g}\hat{T}^{A2g}\{F_{QB}^{\tilde{a}}(\tilde{\nu}_Q, \tilde{\nu}_B) + C_{QB}^{\tilde{a}}F_{QB}^{\tilde{s}}(\tilde{\nu}_Q+\Omega_\mu, \tilde{\nu}_B+\Omega_\mu)\} + \sum_{e,s=Q,B}\left\{\left[\sum_\Gamma \alpha_{es}^\Gamma \hat{T}^\Gamma\right] \times [F_{es}^{\tilde{s}}(\tilde{\nu}_e, \tilde{\nu}_s) + C_{es}^{\tilde{s}}F_{es}^{\tilde{s}}(\tilde{\nu}_e+\Omega_\mu, \nu_s+\Omega_\mu)]\right\} \quad (5)$$

with

$$C_{QQ}^{\tilde{s}} = \frac{\langle 0_\mu^g|1_\mu^Q\rangle\langle 1_\mu^Q|0_\mu^g\rangle}{\langle 0_\mu^g|0_\mu^Q\rangle\langle 0_\mu^Q|0_\mu^g\rangle}$$

$$C_{BB}^{\tilde{s}} = \frac{\langle 0_\mu^g|1_\mu^B\rangle\langle 1_\mu^B|0_\mu^g\rangle}{\langle 0_\mu^g|0_\mu^B\rangle\langle 0_\mu^B|0_\mu^g\rangle}$$

$$C_{QB}^{\tilde{s},\tilde{a}} = \frac{\langle 0_\mu^g|1_\mu^B\rangle\langle 1_\mu^B|1_\mu^a\rangle\langle 1_\mu^Q|0_\mu^g\rangle}{\langle 0_\mu^g|0_\mu^g\rangle\langle 0_\mu^B|0_\mu^Q\rangle\langle 0_\mu^Q|0_\mu^g\rangle} + \tilde{C}_{QB}^{\tilde{s},\tilde{a}}. \quad (6)$$

Ω_μ is the wave number of the phonon participating in the transitions related to the sidebands of Q and B. $|0^g\rangle$ is the vibronic wave function of the electronic ground state with no vibration excited and $|1^e\rangle$ is the vibronic wave function of the electronic state $|e\rangle$ ($e = Q, B$) with our representative vibration excited. $\tilde{C}_{Q,B}^{a,s}$ is a term resulting from the fact that the Q_{01}-band, which becomes optically allowed by vibronic coupling of the Q- and B-state, contributes to Raman scattering. (a, s labels the antisymmetric, symmetric part of C_{QB}.)

Using this first correction of our approach, we are able to fit all obtained oxyHb data. The results of these fits will be discussed later. The main problem in this approach is the necessity to use complex constants α_{es}^Γ, to fit the experimental data.

To clarify this point, we have to take into consideration that the PNSF theory based on Loudon's approach is a strictly time-dependent perturbation theory, including the time-dependence of the photon and phonon field. In our introduction of the extra electronic level associated with the creation of one phonon, we have used a time-independent approach for simplicity. In the formulation of Loudon, however, a fifth-order time-dependent contribution would have been necessary.

Starting from this point of view, we give an extension of the electron-phonon operator H_{EV}, which has been used with the PNSF theory:

$$H_{EV} = \left(\frac{\hbar}{2\pi\Omega_R \cdot C}\right)^{1/2}\frac{\partial H}{\partial Q_R}\Gamma_R(b_R^+ + b_R) + \left(\frac{\hbar}{2\pi\Omega\mu C}\right)^{1/2}\frac{\partial H}{\partial Q_\mu}\Gamma_\mu(b_\mu^+ + b_\mu) \quad (7)$$

Ω_R, Ω_μ: wave number of the Raman-active phonon R, and a non-Raman-active representative phonon μ, which gives rise to the appearance of the Q- and B-sidebands; b_R^+, b_μ^+; b_R, b_μ: creation, annihilation operator of the R-, μ-phonon, respectively. According to Loudon, fifth-order scattering processes can be described by the following transition rate (Loudon 1973)

$$\frac{1}{\tau_5} = \frac{2\pi}{\hbar^2}\left|\frac{1}{C^4\hbar^4}\sum_{l_1}\sum_{l_2}\sum_{l_3}\sum_{l_4}\left(\frac{\langle f|H_I|l_4\rangle\langle l_4|H_I|l_3\rangle}{(\tilde{\nu}_i-\tilde{\nu}_{l4})(\tilde{\nu}_i-\tilde{\nu}_{l3})} \times \frac{\langle l_3|H_I|l_2\rangle\langle l_2|H_I|l_1\rangle\langle l_1|H_I|i\rangle}{(\tilde{\nu}_i-\tilde{\nu}_{l2})(\tilde{\nu}_i-\tilde{\nu}_{l1})}\right)\right|\delta(\tilde{\nu}_i-\tilde{\nu}_f) \quad (8)$$

with

$$H_I = H_{ER} + H_{EV}$$

$$H_{ER} = i\left(\frac{2\pi\hbar}{\nu}\right)^{1/2}\sum_{K,\sigma}(c\cdot\tilde{\nu}_K)^{1/2}[\alpha_{\sigma,k}^+ - \alpha_{\sigma,k}]R_{\sigma,k} \quad (9)$$

$|i\rangle$ ($|f\rangle$) labels the initial (final) states, $|l_1\rangle$, $|l_2\rangle$, $|l_3\rangle$ and $|l_4\rangle$ are the intermediate states of the scattering process. $\tilde{\nu}_i$, $\tilde{\nu}_{l_1} \ldots \tilde{\nu}_{l_4}$ are the total energies of the atomic system in the corresponding status. The δ-function formulates the energy conservation of the process. H_{ER} is the electron-photon interaction operator and contains the dipole-operators $R_{\sigma,k}$ (σ is the polarisation state of the k-th photon) and the creation and annihilation operators for a photon ($\alpha_{\sigma,k}^+$, $\alpha_{\sigma,k}$). $\tilde{\nu}_k$ is the wave number of the k-th photon.

The transition matrix elements are determined by the following wave functions: (n_1, n_2: occupation number of the exciting and scattered photon, respectively v_R, v_μ: occupation number of the Raman phonon

R and the phonon μ, g: electronic ground state; e, s, t, u: excited electronic states.)

$$|i\rangle = |n_1, n_2, \nu_R, \nu_\mu, g\rangle$$

$$|f\rangle = |n_1+1, n_2+1, \nu_R+1, \nu_\mu, g\rangle$$

$$|l_1\rangle_1 = |n_1-1, n_2, \nu_R, \nu_\mu, e\rangle \quad |l_1\rangle_2 = |n_1, n_2+1, \nu_R, \nu_\mu, e\rangle$$

$$|l_2\rangle_1 = |n_1-1, n_2, \nu_R+1, \nu_\mu, e\rangle \quad |l_2\rangle_2 = |n_1, n_2+1, \nu_R+1, \nu_\mu, s\rangle$$

$$|l_2\rangle_3 = |n_1-1, n_2, \nu_R, \nu_\mu+1, s\rangle \quad |l_2\rangle_4 = |n_1, n_2+1, \nu_R, \nu_\mu+1, s\rangle$$

$$|l_3\rangle_1 = |n_1-1, n_2, \nu_R+1, \nu_\mu+1, t\rangle \quad |l_3\rangle_2 = |n_1, n_2+1, \nu_R+1, \nu_\mu+1, t\rangle$$

$$|l_3\rangle_3 = |n_1-1, n_2, \nu_R+1, \nu_\mu+1, t\rangle \quad |l_3\rangle_4 = |n_1, n_2+1, \nu_R+1, \nu_\mu+1, t\rangle$$

$$|l_3\rangle_5 = |n_1-1, n_2, \nu_R, \nu_\mu, t\rangle \quad |l_3\rangle_6 = |n_1, n_2+1, \nu_R, \nu_\mu, t\rangle$$

$$|l_4\rangle_1 = |n_1-1, n_2, \nu_R+1, \nu_\mu, u\rangle \quad |l_4\rangle_2 = |n_1, n_2+1, \nu_R, \nu_\mu, u\rangle \tag{10}$$

$|l_j\rangle_i$, $j = 1, 2 \ldots$, $i = 1, 2 \ldots$ labels different versions of the intermediate state j, defined by an excited electronic state $|e\rangle$, $|s\rangle$. If one introduces Eqs. (6) and (7) into Eq. (5), one obtains after some straightforward calculations the following fifth order contribution to the polarisability tensor.

$$\beta^5_{\sigma\varrho} = \sum_{\substack{e,s \\ =Q,B}} \sum_{t,u} \frac{\hbar^{3/2}}{(2\pi c)^{3/2} \Omega_R^{1/2} \Omega_\mu} \times \left[\left(\frac{\langle g|R_\varrho|e\rangle \langle u|R_\sigma|g\rangle}{(\tilde{\nu}_u - \tilde{\nu}_L + i\gamma^u)} \right) \right.$$

$$\times \left(\frac{\left\langle e \left| \frac{\partial H}{\partial Q^{\Gamma_\mu}} \right| s \right\rangle \left\langle s \left| \frac{\partial H}{\partial Q^{\Gamma_R}} \right| t \right\rangle \left\langle t \left| \frac{\partial H}{\partial Q^{\Gamma_R}} \right| u \right\rangle}{(\tilde{\nu}_e + \Omega_R - \tilde{\nu}_L + i\gamma^e)(\tilde{\nu}_s + \Omega_R + \Omega_\mu - \tilde{\nu}_L + i\gamma^s)(\nu_t + \Omega_R - \tilde{\nu}_L + i\gamma^t)} \right.$$

$$+ \frac{\left\langle e \left| \frac{\partial H}{\partial Q^{\Gamma_\mu}} \right| s \right\rangle \left\langle s \left| \frac{\partial H}{\partial Q^{\Gamma_R}} \right| t \right\rangle \left\langle t \left| \frac{\partial H}{\partial Q^{\Gamma_\mu}} \right| u \right\rangle}{(\tilde{\nu}_e + \Omega_R - \tilde{\nu}_L + i\gamma^e)(\tilde{\nu}_s + \Omega_R + \Omega_\mu - \tilde{\nu}_L + i\gamma^s)(\nu_t + \Omega_\mu - \tilde{\nu}_L + i\gamma^t)}$$

$$\left. \left. + \frac{\left\langle e \left| \frac{\partial H}{\partial Q^{\Gamma_R}} \right| s \right\rangle \left\langle s \left| \frac{\partial H}{\partial Q^{\Gamma_\mu}} \right| t \right\rangle \left\langle t \left| \frac{\partial H}{\partial Q^{\Gamma_\mu}} \right| u \right\rangle}{(\tilde{\nu}_e + \Omega_R - \tilde{\nu}_L + i\gamma^e)(\tilde{\nu}_s - \tilde{\nu}_L + i\gamma^s)(\tilde{\nu}_t + \Omega_R + \Omega_\mu - \tilde{\nu}_L + i\gamma^t)} \right) \right] \tag{11}$$

Antiresonance terms habe been omitted for clarity, but they are regarded in the fitting procedure.

$\tilde{\nu}_u$, $\tilde{\nu}_e$, $\tilde{\nu}_s$, $\tilde{\nu}_t$ are the wave numbers of the electronic transitions into the $|e\rangle$, $|s\rangle$, $|t\rangle$, $|u\rangle$ ($e, s, t, u = Q, B$) excited electronic states and γ^e, γ^t, γ^μ, γ^s, label the corresponding half-widths.

In Eq. (11) all transition moments due to vibronic coupling connecting the ground state to one of the excited electronic states, have been neglected (Albrecht 1960; Peticolas 1970; Collins 1973).

The complete polarisability tensor is given by the sum of the third-order and fifth-order terms. Using a similar notation as in Eq. (3), we obtain the following equation:

$$\beta = \sum_{e,s} \sum_{t,u} \sum_{\mu} \sum_{\underline{P}} M^{ge} M^{ug} \{ (C^{\Gamma_R}_{es} \hat{T}^{\Gamma_R}_{\underline{P}_1}) \times (C^{\Gamma_\mu}_{st} \hat{T}^{\Gamma_\mu}_{\underline{P}_2}) (C^{\Gamma_\mu}_{tu} \hat{T}^{\Gamma_\mu}_{\underline{P}_3}) \}_{\underline{P}} F^{\underline{P}}(\tilde{\nu}_e, \tilde{\nu}_s, \tilde{\nu}_t, \tilde{\nu}_u)$$

$$+ \sum_{e,s} M^{ge} M^{sg} C^{\Gamma_R}_{es} F(\tilde{\nu}_e, \tilde{\nu}_s) . \tag{12}$$

M^{ge}, M^{ug} are the electric dipole matrix elements, connecting the ground state $|g\rangle$ and the excited states $|e\rangle$, $|u\rangle$. The constants $C^{\Gamma_R}_{es}$, $C^{\Gamma_\mu}_{st}$ label the vibronic coupling matrix elements due to the Raman phonon R and the non-Raman-active phonon μ. The sum $\sum_{\underline{P}}$ runs over all permutations

$$P = \begin{pmatrix} 1 & 2 & 3 \\ \underline{P}_1 & \underline{P}_2 & \underline{P}_3 \end{pmatrix} .$$

$F^{\underline{P}}(\tilde{\nu}_e, \tilde{\nu}_s, \tilde{\nu}_t, \tilde{\nu}_u)$ are the frequency functions for each term of this sum, containing energy denominators which describe $|0, 0_R\rangle \rightarrow |0_\mu, 1_e\rangle$, $|0_\mu, 0_R\rangle \rightarrow |1_\mu, 0_R\rangle$ and $|0_\mu, 0_R\rangle \rightarrow |1_\mu, 1_R\rangle$ resonance enhancement. $F_{es}(\tilde{\nu}_e, \tilde{\nu}_s)$ labels the frequency functions of the third-order term (symmetric and antisymmetric). $\hat{T}^{\Gamma_R}$, $\hat{T}^{\Gamma_\mu}$ are McClain tensors due to the representations Γ_R, Γ_μ. The sum $\sum_{\mu}$ runs over all non-Raman-active phonons.

The polarisability tensor β transforms like the product representation $\Gamma^R \times \Gamma^\mu \times \Gamma^\mu = \Gamma^R$ in D_{4h}-symmetry. Therefore in ideal D_{4h}-symmetry no DPR dispersion is introduced into β by the fifth-order terms. However, if one regards symmetry-classified distortions δQ^{Γ_j} of the haem group, the operators $\frac{\partial H}{\partial Q^{\Gamma_R}}$ and $\frac{\partial H}{\partial Q^{\Gamma_\mu}}$ *must be substituted by*

$$\frac{\partial H}{\partial Q^{\Gamma_R}} + \sum_{\Gamma_j} \left(\frac{\partial^2 H}{\partial Q^{\Gamma_R} \partial Q^{\Gamma_j}} \right) \times \delta Q^{\Gamma_j} \quad \text{and}$$

$$\frac{\partial H}{\partial Q^{\Gamma_\mu}} + \sum_{\Gamma_j} \left(\frac{\partial^2 H}{\partial Q^{\Gamma_\mu} \partial Q^{\Gamma_j}} \right) \times \delta Q^{\Gamma_j} .$$

The sum $\sum_{\Gamma_j}$ runs over the irreducible representations A_{1g}, B_{1g}, B_{2g} and A_{2g} of the D_{4h}-symmetry group. This leads to the final expression:

$$\beta = \sum_{e,s}\sum_{t,u}\sum_{\mu}\sum_{\underline{P}}\Big[M^{ge}M^{\mu g}\Big\{\Big(\sum_{j} C_{es}^{\Gamma_{Rj}}\hat{T}^{\Gamma_{Rj}}\Big)_{\underline{P}_1} \times \Big(\sum_{j'} C_{es}^{\Gamma_{j'}}\hat{T}^{\Gamma_{j'}}\Big)_{\underline{P}_2}\Big(\sum_{j''} C_{es}^{\Gamma_{j''}}\hat{T}^{\Gamma_{j''}}\Big)_{\underline{P}_3}\Big\}_{\underline{P}} \times F^{\underline{P}}(\tilde{\nu}_e, \tilde{\nu}_s, \tilde{\nu}_t, \tilde{\nu}_u)\Big] + \sum_{e,s}\Big[M^{ge}M^{sg}\Big(\sum_{j} C_{es}^{\Gamma_{Rj}}\hat{T}^{\Gamma_{Rj}}\Big)F_{es}(\tilde{\nu}_e, \tilde{\nu}_s)\Big] \qquad (13)$$

with perturbation introduced above. Γ_{Rj} contains the representation Γ_R of the Raman mode, $\Gamma_{j'}$, $\Gamma_{j''}$ contain the representation of the μ-th non-Raman-active mode. β transforms like $\Gamma_j \times \Gamma_{j'} \times \Gamma_{j''}$ (Γ_j, $\Gamma_{j'}$, $\Gamma_{j''} = A_{1g}$, B_{1g}, B_{2g}, A_{2g}). This now introduces a variation of the DPR with the excitation wave number.

Using real $C_{es}^{\Gamma_{Rj}}$, $C_{es}^{\Gamma_{j'}}$, $C_{es}^{\Gamma_{j''}}$ as fitting parameters we are now able to fit DPR dispersion curves and EPs simultaneously. For simplicity we use only one representative frequency Ω_μ for the non-Raman-active phonons.

If only one kind of molecule is present in the sample, the fitting constants are linearly related to the static distortions δQ^{Γ_j} of the haem (Eq. 12a). As we will show in the Discussion, different types of molecules with differing distortions exist at a given pH-value between pH = 6.0 and 9.0 due to different titration states of the molecule. In this case the $C_{es}^{\Gamma_{Rj}}$, $C_{es}^{\Gamma_j}$ are effective tensor parameters resulting from incoherent superposition of the Raman intensities due to each type of the molecule. The DPR is calculated using Placzek's formalism (Placzek 1934).

In the following section we discuss the result of the fits for the Raman lines at 1,375 cm^{-1}, 1,583 cm^{-1}, and 1,638 cm^{-1}. A detailed discussion of our new theoretical approach is out of the scope of this paper and will be presented elsewhere.

Experimental

Human adult haemoglobin was prepared from freshly drawn blood by standard procedure described by Schweitzer et al. (1982). The haemoglobin solutions were dialysed against buffer (0.4 M *bis-tris* buffer and 0.4 M *tris* buffer were used for the acid and alkaline pH-range, respectively). The concentration of haemoglobin was determined by measuring optical absorbance.

The excitation was obtained from an Argon-ion laser. The laser beam, polarised perpendicularly to the scattering plane was focussed by a cylindrical lens onto the sample, which was situated in a copper block for cooling (temperature 6° C). The Raman radiation was measured in backscattering geometry. A polarisation analyser between sample and entrance slit of the Czerny Turner double monochromator enabled us to measure the intensity of the two components perpendicular ($I_\perp$) and parallel ($I_\parallel$) to the scattering plane (DPR: $\varrho = I_{\parallel}/I_\perp$). To eliminate the different transmission of the spectrometer for the two components, a polarization scrambler was placed between analyser and entrance slit. To obtain the excitation profiles of Raman lines we have taken into account

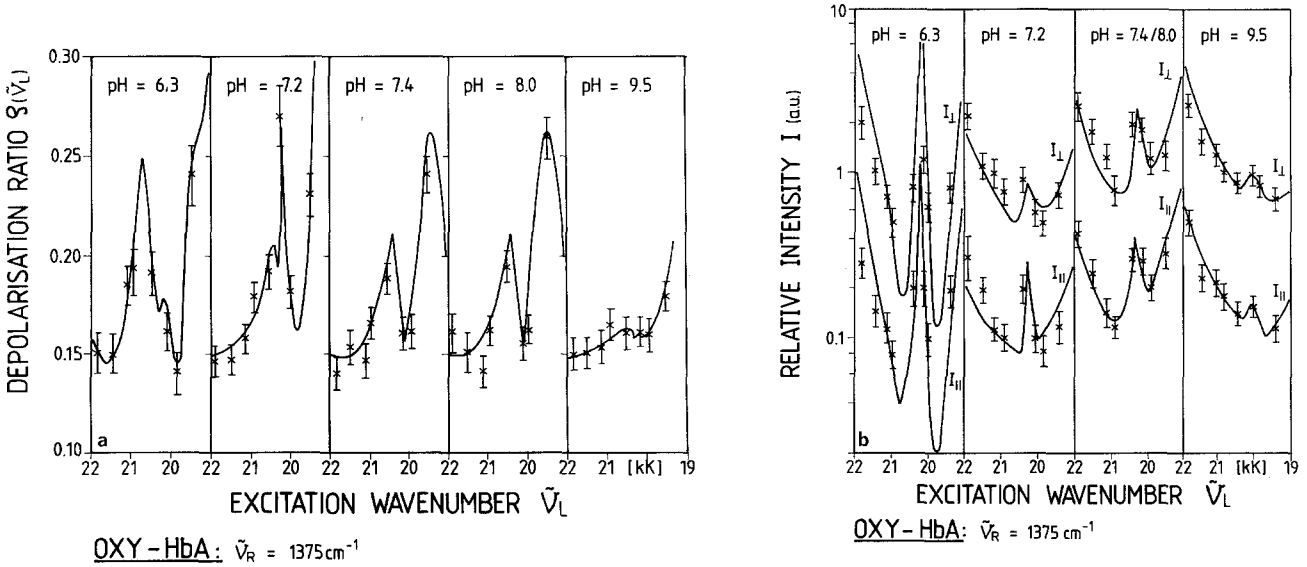

Fig. 1. DPR dispersion curves and EPs curves of the 1,375 cm^{-1} Raman line of the oxyhaemoglobin spectrum for different pH-values of the solution (the full line has been calculated by the fitting procedure)

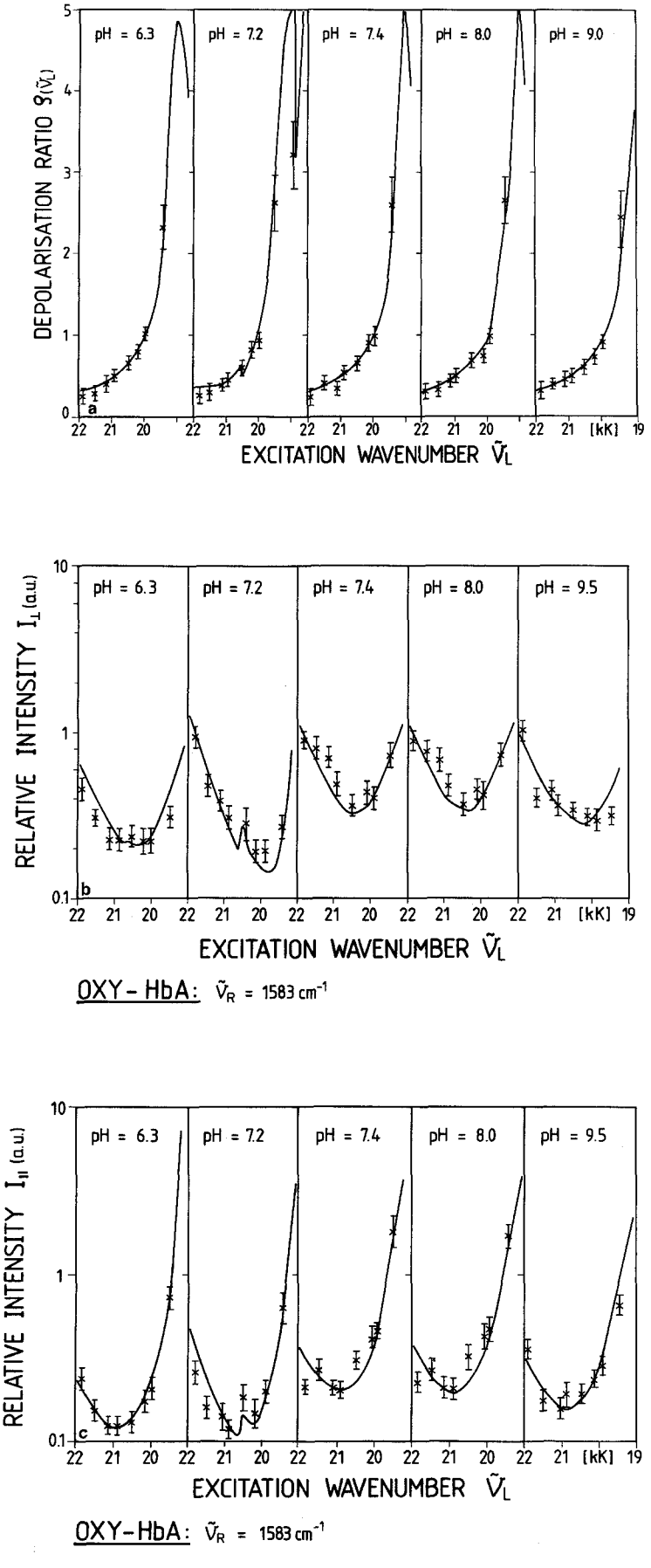

Fig. 2. DPR dispersion curves and EPs curves of the 1,583 cm^{-1} Raman line of the oxyhaemoglobin spectrum for different pH-values of the solution (the full line has been calculated by the fitting procedure)

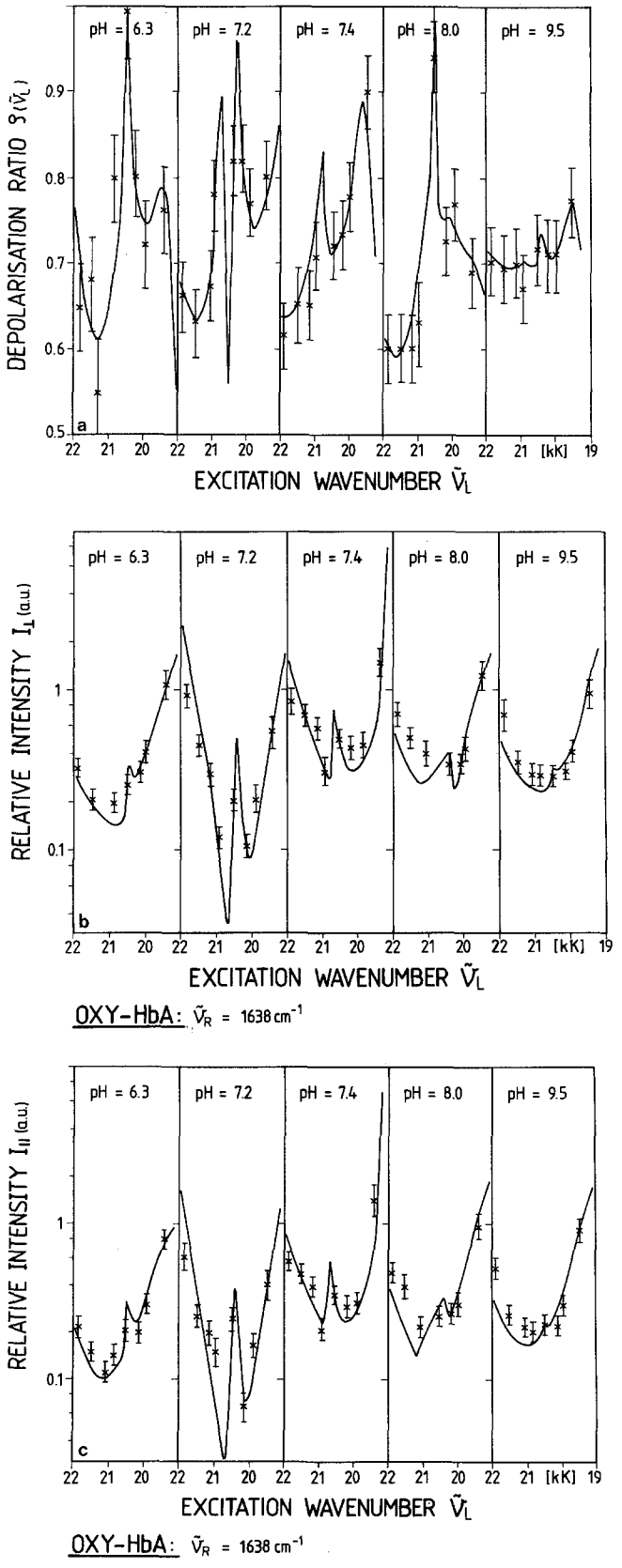

Fig. 3. DPR dispersion curves and EPs curves of the 1,638 cm^{-1} Raman line of the oxyhaemoglobin spectrum for different pH-values of the solution (the full line has been calculated by the fitting procedure)

the transmission dispersion of the analyser and the spectrometer. The transmission of the analyser has been measured with a Cary absorption spectrometer. The transmission of the spectrometer was determined by measuring the Raman intensity of several lines of calcite and quartz, which have frequency-independent Raman tensors for all excitation-wavelengths of the Argon-ion laser and by correcting for the $\tilde{\nu}_R^4$-frequency dependence.

A correction for absorption of the sample is not necessary since the absorption of the solution for the maximal concentration of 10^{-3} mol/monomer is of the order of 8 cm^{-1}. The length of the scattering volume, imaged to the entrance slit is about 100 μm, which is smaller by a factor of 10 than the penetration depth of the exciting radiation into the sample.

Results

Figures 1–3 show the DPR dispersion curves and the corresponding EPs of the 1,375 cm^{-1} (oxidation marker), 1,583 cm^{-1} (spin marker) and the 1,638 cm^{-1} (spin marker) Raman lines of the oxyhaemoglobin spectrum for pH-values between 6.3 and 9.5. The full lines give the results of the fitting procedures. Good agreement was obtained with the experimental data. The results may be classified as follows:

a) The oxidation marker line at 1,375 cm^{-1}

The corresponding mode of this Raman line transforms due to A_{1g} in ideal D_{4h}-symmetry. Therefore, its DPR should be 0.125, if the molecule existed in this ideal symmetry. In reality the DPR varies between 0.13 and 0.27 in the preresonant region between β- and Soret-band. This DPR dispersion is significantly pH-dependent in the physiological region. The corresponding EPs show a maximum at 20,400 cm^{-1}, although there is no absorption band in the optical spectrum, which can be related to $\pi \rightarrow \pi^*$ transitions of the porphyrin system (the z-polarised charge-transfer band at 22,000 cm^{-1} does not contribute to the resonant Raman enhancement of porphyrin skeleton vibrations). To explain these effects, one has to regard static distortions δQ^{Γ_j} of the haem and the contribution of a second, non-Raman-active phonon. We have shown (theoretical background) that by fitting the experimental data to Eq. (13) one obtains constants $C_{es}^{\Gamma_{Rj}}$, $C_{es}^{\Gamma_j}$, which are related to symmetry classified distortions of the haem group, affecting the Raman vibration and the μ-th vibration, respectively. From the representation Γ_R of the Raman line in ideal D_{4h}-symmetry and the corresponding symmetry Γ_{Rj} of the tensor parameter $C_{es}^{\Gamma_{Rj}}$,

Table 1. $c_{es}^{\Gamma Rj}$, $c_{es}^{\Gamma j'}$, values of the 1,375 cm^{-1} Raman line of the oxyhaemoglobin spectrum calculated by the fitting procedure

Parameter		pH				
		6.3	7.2	7.4	8.0	9.5
C^{A1gR}	QQ	9.18	−2.72	0.89	0.89	−1.42
	QB	4.85	2.10	0.30	0.30	−2.12
	BB	2.25	0.40	0.49	0.49	1.57
C^{B1gR}	QQ	−11.4	–	−0.49	−0.49	0.31
	QB	0.68	–	0.23	0.23	0.13
	BB	0.73	–	−0.089	−0.089	0.18
C^{B2gR}	QQ	1.81	4.37	−0.61	−0.61	−0.57
	QB	–	1.12	–	–	–
	BB	− 0.62	−0.26	−0.16	0.16	0.71
C^{A1g}	QQ	0.183	−0.15	0.94	0.94	0.42
	QB	0.37	0.79	0.50	0.50	−0.08
	BB	0.36	0.63	0.03	0.03	0.074
C^{B1g}	QQ	0.24	−0.6	−0.28	−0.28	0.329
	QB	0.06	−0.09	0.20	0.20	−0.15
	BB	− 0.42	−0.07	0.43	0.43	−0.002
C^{B2g}	QQ	0.01	−0.03	0.59	0.59	−0.015
	QB	0.15	−0.09	0.18	0.18	0.06
	BB	0.31	0.89	−0.56	−0.56	0.33
Ω_μ		1,551	1,551	1,551	1,551	1,551
γ^Q (cm^{-1})		500	500	500	500	500
γ^B						

Table 2. $c_{es}^{\Gamma Rj}$, $c_{es}^{\Gamma j'}$, values of the 1,583 cm^{-1} Raman line of the oxyhaemoglobin spectrum calculated by the fitting procedure

Parameter		pH				
		6.3	7.2	7.4	8.0	9.5
C^{A1gR}	QQ	–	–	–	–	–
	QB	–	–	–	–	–
	BB	0.16	0.17	0.17	0.17	0.14
C^{B1gR}	QQ	–	–	–	–	–
	QB	–	–	–	–	–
	BB	–	–	–	–	–
C^{B2gR}	QQ	3.76	3.92	−3.6	−3.6	3.15
	QB	0.18	0.25	0.18	0.18	0.15
	BB	0.15	0.20	0.15	0.15	0.12
C^{A2gR}		0.25	0.26	0.24	0.24	0.20
C^{A1g}	QQ	0.183	−0.15	0.94	0.94	0.42
	QB	0.37	−0.75	0.50	0.50	−0.08
	BB	0.36	0.63	0.03	0.03	0.074
C^{B1g}	QQ	0.24	−0.6	−0.28	−0.28	0.329
	QB	0.06	−0.09	0.20	0.20	−0.15
	BB	−0.42	−0.07	0.43	0.43	−0.002
C^{B2g}	QQ	0.01	−0.03	0.51	0.51	−0.015
	QB	0.15	−0.09	0.18	0.18	0.06
	BB	0.31	0.89	−0.56	−0.56	0.33
Ω_μ		1,551	1,551	1,551	1,551	1,551
γ^Q (cm^{-1})		500	500	500	500	500
γ^B						

Table 3. $c_{es}^{\Gamma_{Rj}}$, $c_{es}^{\Gamma_{j'}}$, values of the 1,638 cm^{-1} Raman line of the oxyhaemoglobin spectrum calculated by the fitting procedure

Parameter		pH				
		6.3	7.2	7.4	8.0	9.5
C^{A1gR}	QQ	5.6	3.06	− 9.77	− 0.84	0.32
	QB	4.35	−0.36	0.86	0.21	−1.51
	BB	0.15	−0.30	0.57	0.36	0.23
C^{B1gR}	QQ	–	4.28	–	–	–
	QB	4.2	−0.24	2.41	6.06	2.77
	BB	1.86	0.34	2.20	0.37	−0.47
C^{B2gR}	QQ	48.7	3.42	17.98	16.84	0.15
	QB	–	0.61	1.42	0.013	–
	BB	–	0.19	2.18	2.91	1.49
C^{A1g}	QQ	0.183	−0.15	0.94	0.94	0.42
	QB	0.37	0.79	0.5	0.5	−0.08
	BB	0.36	0.63	0.03	0.03	0.074
C^{B1g}	QQ	0.24	−0.6	− 0.28	− 0.28	0.329
	QB	0.06	−0.09	0.20	0.20	−0.15
	BB	0.42	−0.07	0.43	0.43	−0.002
C^{B2g}	QQ	0.01	−0.03	0.59	0.59	−0.015
	QB	0.15	−0.09	0.18	0.18	0.06
	BB	0.31	0.89	− 0.50	− 0.56	0.33
Ω_μ		1,551	1,551	1,551	1,551	1,551
γ^Q (cm^{-1})		500	500	500	500	500
γ^B						

one obtains the representation of these distortions (Schweitzer-Stenner et al. 1984) (cf. theoretical background).

To obtain comparable values for the constant $C_{es}^{\Gamma_{Rj}}$, $C_{es}^{\Gamma_{j'}}$, we calculate the vibronic coupling matrix of Eq. (11) in units of $(\hbar/2\,\pi c\Omega_e)^{1/2}$ and $(\hbar/2\,\pi c\Omega_\mu)^{1/2}$. The dipole matrix elements are calculated from the oscillator strengths given by Hsu and Woody (1971) to $Mg_B = 7.2$ Debye for the Soret- and $Mg_Q = 0.6$ Debye for the α-transition.

From the fitting procedure we deduce that $C_{es}^{\Gamma_{Rj}}$, $C_{es}^{\Gamma_{j'}}$ with $\Gamma_{Rj} = A_{1g}, B_{1g}, B_{2g}$ and $\Gamma_{j'} = A_{1g}, B_{1g}, B_{2g}$ contribute to the scattering tensor at all pH-values (Table 1). Therefore, one can conclude that B_{1g} and B_{2g} distortions affects the vibration of this mode.

The constants $C_{es}^{\Gamma_{j'}}$ of the μ-th non-Raman-active phonon are in the same order of magnitude as the corresponding $C_{es}^{\Gamma_{Rj}}$. From the fitting procedure we obtain a representative frequency $\Omega_\mu = 1{,}551$ cm^{-1}. This is the wave number of a B_{1g}-mode of the oxyhaemoglobin Raman vibrations (Abé et al. 1978; Spiro and Strekas 1974). The fact that we observe large B_{1g} contributions to $C_{es}^{\Gamma_{j'}}$ is a good reference as to the consistency of our fit.

The calculated electronic half-width of 500 cm^{-1} is in the order of magnitude of the experimental values of the Soret- and the α-band.

b) The spin marker line at 1,583 cm^{-1}

If the haem group has an ideal D_{4h}-symmetry, the DPR of this line would be due to an A_{2g} mode. In the region from 22,000 cm^{-1} to 21,000 cm^{-1} the Raman radiation is polarised, anomalously polarised radiation is observed with a steep increase in DPR up to 2.5. Although the DPR dispersion is almost insensitive to the pH-value, the EPs are pH-dependent.

$C_{es}^{\Gamma_{Rj}}$ constants with $C_{es}^{\Gamma_{Rj}} = A_{1g}, A_{2g}$ and B_{2g} contribute to the scattering tensor at all pH-values. The constants $C_{es}^{\Gamma_{j'}}$, which are related to coupling with the non-Raman-active phonon, are equal in magnitude to those obtained from the 1,375 cm^{-1} line.

c) The spin marker line at 1,638 cm^{-1}

This line corresponds to a B_{1g} mode in D_{4h}-symmetry. Thus, the line should be depolarised (DPR = 0.75). The DPR, however, shows a drastic dispersion in the preresonant region (DPR = 0.5−1) and a strong influence of the pH-value in the physiological region. $C_{es}^{\Gamma_{Rj}}$, $C_{es}^{\Gamma_{j'}}$ constants with $\Gamma_{Rj}, \Gamma_{j'} = A_{1g}, B_{1g}$ and B_{2g} are needed to fit the DPR and EPs of this line for all pH-values. Again all $C_{es}^{\Gamma_{j'}}$-constant are equal magnitude to those of the oxidation marker line and the spin marker line at 1,583 cm^{-1}.

The fact that the fitting constants, which contain the coupling to the non-Raman-active phonon, are *equal in magnitude for all three lines* observed at each pH is extremely important and shows the consistency of our theory.

In Eq. (12) these coupling elements represent the interaction with the non-Raman-active phonon and thus their values are independent on the Raman phonon observed in agreement to what we have obtained. This also reduces the effective number of fitting parameters needed.

Discussion

1. Parameter $C_{es}^{\Gamma_{Rj}}$ related to static distortions of the molecules

From the fitting parameters $C_{es}^{\Gamma_{Rj}}$ one obtains the following symmetry-classified distortions of the three Raman modes using the correlation table described in our previous paper (Schweitzer-Stenner et al. 1984).

1,375 cm^{-1}: A_{1g}, B_{1g}, B_{2g} distortions
1,583 cm^{-1}: A_{1g}, A_{2g}, B_{1g} distortions
1,638 cm^{-1}: A_{1g}, A_{2g}, B_{1g} distortions .

This reflects a haem symmetry of C_2 or C_s. At first sight it is an astonishing fact that no A_{2g}-distortions exist for the 1,375 cm^{-1}, and no B_{2g} distortions for the 1,583 cm^{-1} (1,638 cm^{-1}). One has to observe, however, that the vibronic coupling elements $\left\langle e\left|\frac{\partial^2 H}{\partial Q^{\Gamma_R}\partial Q^{\Gamma_j}}\right|s\right\rangle$ depend on the combination of R and j and thus can have differing values.

If one regards the representation of the normal coordinates in cartesian space (Abé et al. 1978) one realises that for most of the atoms the displacement of the A_{2g} and B_{2g} modes are perpendicular to those of the A_{1g}, A_{2g} (B_{1g}) modes in D_{4h}-symmetry, respectively. First considerations have shown that for these combinations the matrix elements $\left\langle e\left|\frac{\partial^2 H}{\partial Q^{\Gamma_R}\partial Q^{\Gamma_j}}\right|s\right\rangle$ should be significantly smaller than for all the other combinations. This agrees well with the data obtained. A detailed discussion will be given in a future paper.

It is remarkable that for all three Raman lines relatively large contributions from $C_{BB}^{B_{2g}^R}$ are obtained. Shelnutt et al. (1977) have calculated the dispersion of DPR and EPs from a different point of view. Regarding vibronic coupling, they first calculate the eigenstates and energies of the system by time-independent theory in third order.

Thus, they take into account Jahn-Teller coupling. The Raman tensors are then calculated by using second-order time-dependent Kramers-Heisenberg formulation. They show that only B_{1g} and B_{2g} modes are Jahn-Teller active. This fact is well reflected in our differently formulated approach by the magnitude of the corresponding $C_{BB}^{B_{2g}^R}$ parameters.

2. Correlation between Bohr effect and haem distortion

Figures 4–6 show the $C_{es}^{\Gamma_{Rj}}$, $C_{es}^{\Gamma_j}$ dependence on the pH-value of the solution for all three Raman lines that we have investigated. One obtains a similar shape for the $C_{es}^{\Gamma_{Rj}}$ (pH) diagrams of the 1,375 cm^{-1} and the

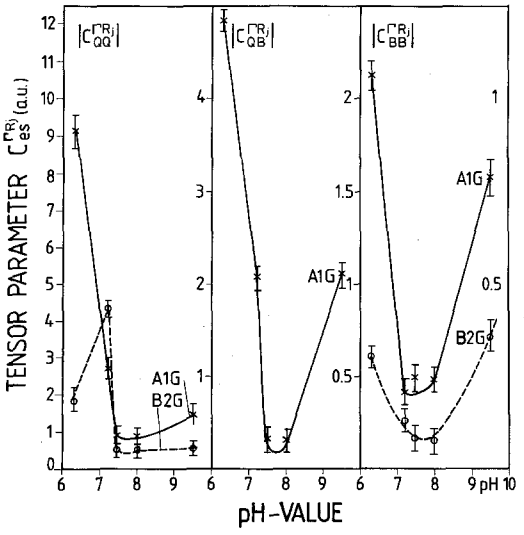

Fig 4. $|C_{es}^{\Gamma_{Rj}}|$ (pH) diagrams of the 1,375 cm^{-1} Raman line of the oxyhaemoglobin spectrum

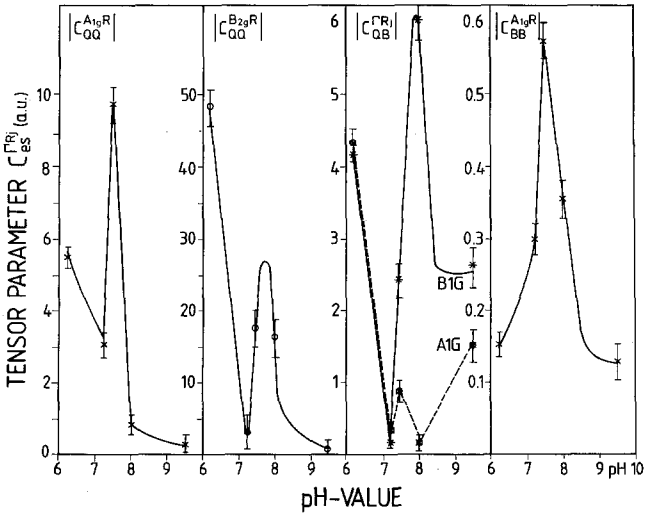

Fig. 5. $|C_{es}^{\Gamma_{Rj}}|$ (pH) diagrams of the 1,638 cm^{-1} Raman line of the oxyhaemoglobin spectrum

1,638 cm^{-1} and for the corresponding $C_{es}^{\Gamma_j}$ (pH) diagrams, i.e., a minimum or a maximum in the region between pH = 7.0 and 8.0. In the acid region some parameters increase or decrease towards pH = 6.0.

It is interesting to note that all $C_{es}^{\Gamma_{Rj}}$ parameters of the 1,375 cm^{-1} Raman line are minimal between pH = 7.0 and 8.0, reflecting a more relaxed state of the haem-apoprotein interaction. The corresponding $C_{es}^{\Gamma_{Rj}}$ parameters of the 1,638 cm^{-1} Raman line, however, show a strong maximum in this region. This is a reference to a strong haem-apoprotein interaction.

To clarify this point, one has to remember that those Raman lines are due to different normal modes of the porphyrin system. From the normal coordinate analysis of Abé et al. (1978) one can deduce that the corresponding mode of the oxidation marker line is due to a pyrrole ring breathing – like mode deformed by large contributions of the CN-stretching vibration. The 1,638 cm^{-1} spin marker line, however, is due to stretching modes of the β-atoms of the pyrrole rings and C-atoms of the side chains. From this one can conclude that haem-apoprotein interactions, which effect the pyrrole rings of the haem, are indicated by the 1,638 cm^{-1} Raman line (Fig. 5). In contrast to this, interactions between the four nitrogen atoms and the proximal or distal histidine can affect the mode of the 1,375 cm^{-1} Raman line (cf. el Naggar et al. 1984; Warshel and Weiss 1982). Therefore, our data can be interpreted by assuming an increase of the van-der-Waals interaction between haem and apoprotein and a simultaneously decrease of the *N*-histidine interaction with changing pH.

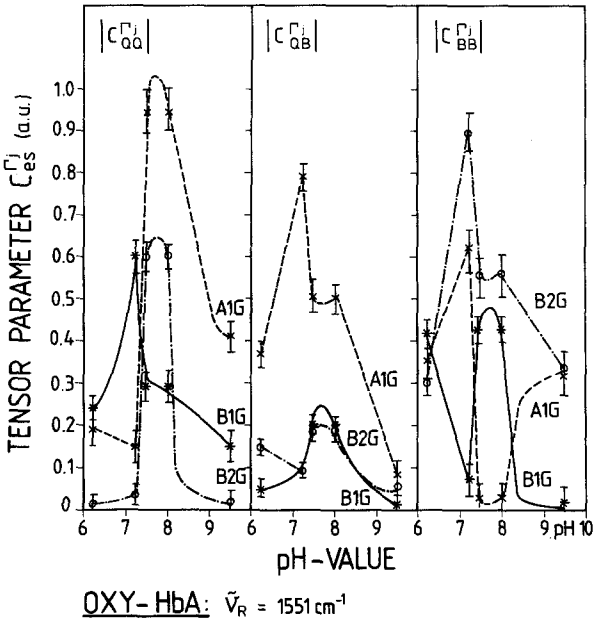

Fig. 6. $|C_{es}^{\Gamma_{Rj}}|$ (pH) diagrams of the different non-Raman-active contribution of the frequency Ω_μ = 1,551 cm^{-1}

If this interpretation is correct, one would expect that the pH-dependence of the 1,583 cm^{-1} Raman line (Fig. 7) should be some order of magnitude smaller than those of two other lines. This mode (Abé et al. 1978) is determined by large vibrations of the methine bridges, which are not in a strong van-der-Waals contact to the globular protein (Antonini and Brunori 1971), and thus should not be very much influenced by changes of protein environment. Therefore, only small variations of the corresponding distortions are to be expected. This is in agreement with the behaviour of the $C_{es}^{\Gamma_{Rj}}$ in Fig. 7.

Although our data reflect different behaviour of the haem-apoprotein interaction, one has to assume a common reason for all these effects. The significant correlation in all diagrams $C_{es}^{\Gamma_{Rj}}$ (pH) and $C_{es}^{\Gamma_j}$ (pH) is the correlation with the alkaline Bohr effect. Between pH = 7.0 and 8.0 the number of protons released, when the system in oxygenated, has a maximum. Therefore, one may ask whether protonation/deprotonation of Bohr groups causes the pH-dependent symmetry distortions of the haem.

In a previous paper (Schweitzer-Stenner et al. 1984) we interpreted similar diagrams of the deoxy-

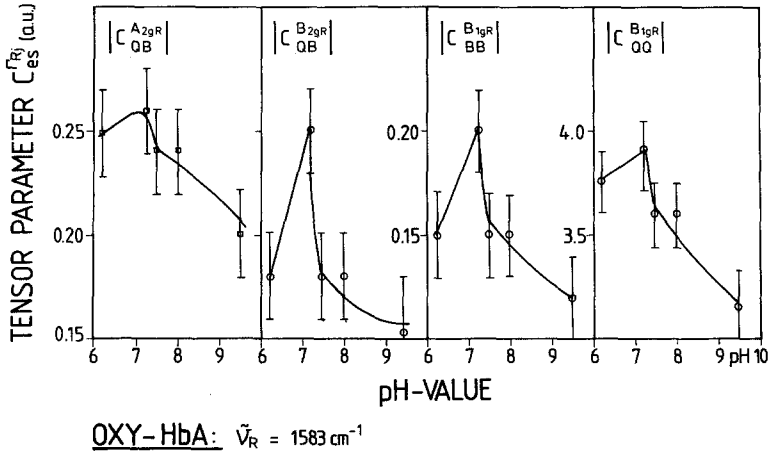

Fig. 7. $|C_{es}^{\Gamma_{Rj}}|$ (pH) diagrams of the 1,583 cm^{-1} Raman line of the oxygaemoglobin spectrum calculated by a fitting procedure, which is based on an approach in third-order time-dependent theory (Schweitzer 1983; Schweitzer et al. 1983)

haemoglobin system by assuming that different titration states of amino acids residues induce different distortions of the haem group. These different kinds of molecules with respect to the distortions and titration state are present in the solution at a given pH-value. The different titration states can be represented by $S_1 = (\underset{1}{+}, \underset{2}{+}, -, \underset{i}{-}, \cdots)$.

(+ means that a proton is bound to the Bohr group, − means that a proton has been released, i labels the number of Bohr groups, 1 the titration state of the molecule.) In each state S_1 different distortions $\delta Q_l^{\Gamma_j}$ exist. The number n_1 of each kind of molecules can be calculated by mass action law as a function $n_1(K_1, K_2, \ldots, K_i, \text{pH})$, where K_i is the corresponding mass action constant. Therefore, the $C_{es}^{\Gamma_{Rj}}$, $C_{es}^{\Gamma_{j'}}$ reflect effective scattering tensor contributions, which result from incoherent superposition of the Raman intensities due to each type of molecule. From the fact that the excitation profiles are only dependent on the squares of Placzek's tensor invariants β^a, β^s and γ^2 respectively (cf. Placzek 1934), one can conclude by some lengthy calculation that all $C_{es}^{\Gamma_{Rj}}$, $C_{es}^{\Gamma_{j'}}$ can be separated by comparing the energy denominators. From this one obtains:

$$C_{es}^{\Gamma} = \begin{cases} \left\{\sum_{l=1}^{4} \frac{n_l}{N}\left[\left(\eta_{es}^{\Gamma,l}\delta Q_l^{\Gamma_j}\right)^2 + \left(\varepsilon_{es}^{\Gamma_{R,l}}\right)^2\right] + \left(\eta_{es}^{\Gamma_u}\varepsilon_{es}^{\Gamma_{R,l}}\delta Q_l^{\Gamma_j}\right) \right. & \begin{matrix}(\Gamma = \Gamma^R)\\(\Gamma = \Gamma^\mu)\end{matrix} \\ \left\{\sum_{l=1}^{4} \frac{n_l}{N}\left(\eta_{es}^{\Gamma,l}\delta Q_l^{\Gamma_i}\right)^2\right. & (\Gamma \neq \Gamma^R \neq \Gamma^\mu)\,, \end{cases} \qquad (14)$$

where

$$\eta_{es}^{\Gamma,e} = \alpha\left\langle s\left|\frac{\partial^2 H}{\partial Q_l^{\Gamma_R}\partial Q_l^{\Gamma_j}}\right|e\right\rangle, \; \varepsilon_{es}^{\Gamma,e} = \beta\left\langle s\left|\frac{\partial H}{\partial Q_l^{\Gamma_R}}\right|e\right\rangle,$$

α, β: constants.

Assuming two titrable groups influencing the haem, we are able to fit the α_{es}^{Γ} (pH) diagrams of the 1,355 cm^{-1} line of the deoxyhaemoglobin spectrum (Schweitzer-Stenner et al. 1984). Unfortunately, the oxy-$C_{es}^{\Gamma_{Rj}}$ (pH) ($C_{es}^{\Gamma_{j'}}$ (pH) diagrams cannot be explained by such a simple approach. Therefore more than two protonation processes may contribute to the variation of the fitting parameters, i.e. the variation of the symmetry-classified distortions of the functional group. The corresponding pH-values lie in the region between 7.0 and 8.0.

If this interpretation is correct, one must conclude that the tertiary structure of the R-state of haemoglobin is pH-dependent. The pH-influence on the R-state properties of haemoglobin has been discussed in the past from many points of view. In terms of the two-state model of Monod et al. (1965), one assumes only pH-variation of the equilibrium constant of the R-T transition to explain the Bohr effect. NMR measurements of the γ_1 and γ_2 Val(E11) methyl resonances, however, show a significant influence of the pD-value on the position of Val(E11) resonance lines which is explained by changing haem-apoprotein contacts (Lindstrom and Ho 1973). Kinetic studies by McDonald and Noble (1972) have demonstrated that the ligand dissociation rate is reduced within the R-form of haemoglobin, when pH is increased from 6 to 9. Consequently new allosteric models have been developed (Herzfeld and Stanley 1974), which take into account pH-dependence of the R-state O_2-affinity. Yassin and Fell (1982) use the Herzfeld-Stanley model to analyse the pH-dependence of oxygen binding of human blood. From their fitting procedures they deduce that H^+-ions directly influence the tertiary structure of the globular structure. In our model this change of oxygen affinity may be caused by the pH-dependent distortions of the haem group.

One interesting result of the studies by McDonald and Noble (1972) should be emphasised. Studying the pH-dependence of CO-dissociation with NO-replacement for HbA and its isolated subunits, they obtain different pH-effects on the rates of CO replacement by NO for the different aggregation states (tetramer, monomer) of the molecule. The pH-effect of the β-subunit has a significant maximum at pH = 8.0 and increases towards the acid region. This corresponds well to the feature of our C_{es}^{Γ} (pH) diagrams. The α-subunit, however, shows only a small pH-dependence of the CO-dissociation/NO-replacement. From this one may conclude that protonation processes of the β-subunit are responsible for the pH-variations of the polarisability tensor as obtained from our data.

Now the question arises as to which amino acid groups of the β-subunit contribute to this effect. Perutz (1970b) has shown that Val(NA1)β, His(HC3)β and His(H5)α are the main causes for the Bohr effect. Matthew et al. (1979a, b) have pointed out that the contributions to the Bohr effect depend on the electrostatic properties of the molecule and the Cl^--concentration of the solution. They calculate relatively large contributions of single groups as Val(NA1)α, Val(HC1)β, and His(HC3)β to the alkaline Bohr effect at a Cl^--concentration of 0.1 M. In the absence of Cl^--ions, however, many additional groups in the − and β-subunits contribute to the Bohr effect in the alkaline region. Results of NMR measurements of the pH-dependence of different $C2$, $C4$ histidyl resonances (Russu et al. 1982), are in good agreement with the theoretical calculations of Matthew et al. (1979b). They find that in the case of low Cl^--concentration the salt bridge between His(HC3)β and Asp(FG1)β remains unchanged in the T-R transition

of the tetramer molecule. This astonishing result is contrary to the interpretation of X-ray diffraction studies of human and horse haemoglobin by Perutz (1970a) and Kilmartin et al. (1980), who did not find this salt bridge in horse oxyhaemoglobin and human methaemoglobin systems. This discrepancy can be explained in terms of Matthews' theory, assuming a fluctuation of the local environment of amino acid residues in dependence of ionic strength and pH-value.

From this state of the discussion two possible explanation may be given for our results. Both represent extreme views from different standpoints. The truth might well be a compromise between the two.

1) Under our condition of low-phosphat and Cl^--concentrations in the range between 0.2 and 0.25 M the salt bridge between His(*HC*3)β and Asp(*FG*1)β may not be destroyed in the *R*-state.

Thus, a deprotonation of His(*HC*3)β can now destabilise this bridge. This would produce a change in the tertiary structure, influencing the haem group and the ligation affinity of this subunit and therefore the polarisability tensor. Russu et al. (1982) measured a pK-value of 7.85 for the His(*HC*3)β residue at low Cl^-- and phosphat-concentrations. Thus, at this pK-value one would expect breaking of the salt bridge in accordance with our diagrams. If this interpretation is correct, the pH-dependence of the polarisability tensor must be absent for systems lacking this salt bridge. Indeed, the corresponding Raman lines of deoxyMb, metMbCN and metHbCN (in the ferric state the salt bridge is absent (Russu et al. 1982; Perutz 1970a; Heidner et al. 1976), show no pH-dependent variation of the DPR and EPS curves (el Naggar et al. 1984).

In the meantime we have investigated the DPR and EPs curves of oxyhaemoglobin Raman lines at high Cl^--concentrations (= 0.45 M). We have found only small variations in the DPR and EPs of the 1,375 cm^{-1}, 1,584 cm^{-1} and 1,638 cm^{-1} Raman line (to be published in a future paper). These results confirm the above interpretation.

Thus, we may conclude that breaking of this salt bridge is a major reason for distortion being induced into the *R*-state. We have to point out, however, that there has be at least one additional titration process with pK in the region between 7 and 8. Otherwise maxima of the $C_{es}^{\Gamma_{Ri}}$ would not be obtained, since from titration of only one residue and its corresponding changes in tertiary structure one would expect normal titration curves without any maxima. Which of the various amino residues takes this role remains to be answered.

It should be noted that a similar "induced fit" effect by breaking of salt bridges has been obtained by Möβbauer's spectroscopy of the monomeric haemoglobin *Chironomos Tummi Tummi* by Parak and Kalvius (1982).

2) Another explanation can be given, if one assumes that the protonation/deprotonation of *all* Bohr groups gives rise to pH-dependent variations of the scattering tensor. Matthew et al. (1970a) have shown that such processes change the electrostatic interactions between different residues of the tetrameric molecule and correspondingly the tertiary structure and the dynamic properties (Frauenfelder et al. 1979). The fact that the $C_{es}^{\Gamma_{Ri}}$ (pH) maximum correlates with the maximum of deprotonation processes of the oxy-system in the alkaline region (Fig. 7) support this interpretation. The absence of a pH-dependent DPR variation of myoglobin Raman lines can be explained in terms of Matthews theory by the more belanced electrostatic interaction pattern in myoglobin apoprotein.

Further experiments, i.e., the investigation of the influence of Cl^--ions and effectors on the DPR and EPs of oxyhaemoglobin are necessary to clarify as to how the two mechanisms proposed really do contribute.

3. Pathways of the haem-apoprotein interaction

We now discussed the mechanism which couples the protonation/deprotonation of Bohr groups and the symmetry distortions of the haem group. The haem-apoprotein interactions have been discussed by several authors during the past few years in the context of ligation processes. Of course, one can assume that ligation and protonation processes trigger haem-apoprotein interaction via the same pathways. Therefore, it seems to be useful to outline the two most important modes of haem-apoprotein interaction. After this, we discuss whether our results favour one of these models.

Wymann (1966) has measured free energy difference between the *R*- and *T*-state of the haemoglobin tetramer. Perutz et al. (1972) assume that this energy is stored in the covalent Fe^{2+}-His(*F*8) bond between haem and globular protein. In the *T*-state the central Fe^{2+}-atom is about 0.4 Å out of the haem plane (model I). In the case of a *T-R* transition, the Fe^{2+}-atom moves towards the haem plane, weakening the Fe^{2+}-His(*F*8) bond. Raman measurements of Nagai et al. (1980) and Ondrias et al. (1982), who have measured a frequency shift of the 212 cm^{-1} Raman line of the deoxyhaemoglobin spectrum during a *T-R* transition of the system, support this theory. Assuming this line to be caused by a Fe-His(*F*8) vibration, they conclude a dominant role of the Fe-His (*F*8) bond in the *T-R* transition. However, up to now this assignment of the 212 cm^{-1} line is not unambiguous (Debois et al. 1981).

The allosteric model of Hopfield (1973) gives another explanation. Hopfield assume that the free

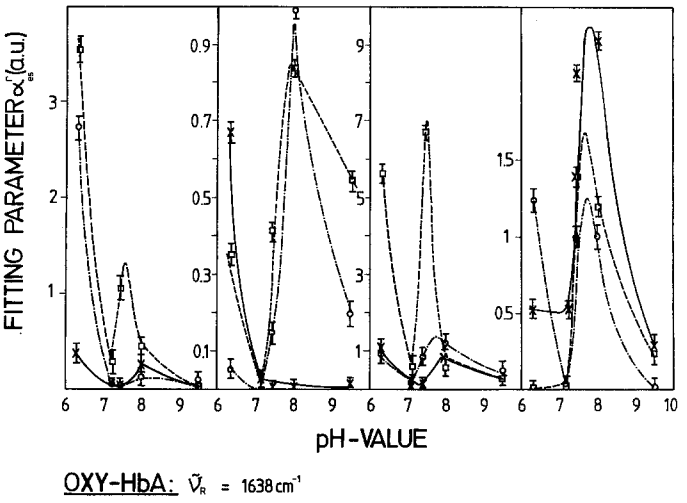

Fig. 8. $|\alpha_{es}^{\Gamma}|$ (pH) diagrams of the 1,683 cm^{-1} Raman line of the oxyhaemoglobin spectrum

energy is distributed evenly over all chemical bonds, i.e., covalent, hydrogen and van der Waals bonds, of the tetrameric molecule. In this case the Fe-His($F8$) bond is not the only pathway of haem-apoprotein interaction, but the van der Waals and hydrogen bonds between the haem-pyrrole rings and amino acid residues of the haem pocket have to be taken into account.

Hopfield's model is supported by the EXAFS measurements of Eisenberger et al. (1976, 1978) and Shulman et al. (1982). Eisenberger et al. (1978) have measured the Fe^{2+}-His($F8$) distance for deoxy-HbA (T-state) and deoxyHb Kempsey (R-state). They found no difference between these two systems. In addition, EXAFS measurements at HbNO in the R- and T-state of Shulman et al. (1982) give no indication for a prominent role of the Fe^{2+}-His($F8$) bond R-T transition.

In an earlier paper, Lindstrom and Ho (1973) showed that the position Val($E11$) influences the ligation affinity of haemoglobin. This interaction is dependent on the pD-value of the solution and on the presence of DPG. Shelnutt et al. (1981) report that Raman difference measurements at different cytochromic mutants which differ in various amino acid residue give rise to small shifts of the spin marker Raman lines. This indicates haem-apoprotein interactions via many different pathway in the protein.

Now the question arises as to whether our experimental results favour one of those two models. In the last section we have shown that the behaviour of the $C_{es}^{\Gamma_{Ri}}$ (pH) diagrams of the 1,375 cm^{-1} and 1,638 cm^{-1} Raman line can be explained by a haem-apoprotein interaction via van der Waals contacts and histidine($F8$,$E7$)-N(porphyrin) interaction. If tertiary structure variation couples to the haem mainly via the covalent Fe^{2+}-His($F8$) bond, one would expect A_{1g}, B_{1g} and B_{2g} distortions of the four nitrogen atoms. This would influence mainly the 1,375 cm^{-1} Raman line. For the 1,638 cm^{-1} Raman mode one would expect a somewhat smaller pH-dependence of the scattering tensor, contrary to what we have obtained.

The model of Hopfield, however, predicts that tertiary structure variation influence the haem with comparable strength via the Fe^{2+}-His($F8$), van der Waals and hydrogen bonds. In this case all modes of the porphyrin system are distorted in a similar way. This is what we have obtained and thus our results support Hopfield's model.

4. Comparison of third-order and fifth-order formalism of the polarisability tensor

In a previous paper we reported that the DPR dispersion curves and EPs of the 1,355 cm^{-1} Raman line of deoxyHb can be calculated with a theoretical approach in third-order time-dependent theory using complex fitting constants α_{es}^{Γ}. From this we obtain several diagrams of α_{es}^{Γ} (pH), which could be explained by protonation/deprotonation of two Bohr groups with pK = 5.4 and 4.3. To clarify the validity of this earlier approach, we compare the results presented in this paper with those we obtained previously by the application of the third-order approach (Eq. (1) in this paper) to oxyHb Raman lines (Schweitzer et al. 1983). Figure 7 shows the pH-dependence of the complex α_{es}^{Γ} of the 1,638 cm^{-1} Raman line of oxyHb spectrum as a representative example. It show a similar behaviour to those diagrams we have presented in this paper (Figs. 4–6). From this similarity one can conclude that both theories yield equivalent results, i.e., the same pH-dependence of static distortions of the haem group. The fifth-order approach, however, avoids some inconsistence of the calculated results as complex transition moments and small electronic half-width of the Q-transition.

We summarise our results as follows:

1) Symmetry-lowering of the functional group oxyhaemoglobin can be detected by measuring and analysing the DPR dispersion curves and EPs of prominent Raman lines.
2) Protonation of Bohr groups with pK-values between 7.0 and 8.0 induces distortions of the haem group via the haem-apoprotein contacts.
3) The similar pH-dependence of all symmetry-classified distortions of the haem supports the distributed model of Hopfield.

Acknowledgement. We would like to thank Prof. Dr. A. Mayer for helpful discussions and Mr. G. Ankele for technical assistance.

References

Abé M, Kitagawa T, Kyogoku Y (1978) Resonance Raman spectra in octaethylporphyrin – Ni (II) and meso-deuterated and ^{15}N substituted derivatives. II. A normal coordinate analysis. J Chem Phys 69: 4526–4534

Alben IO, Bare GH (1980) Ligand-dependent heme-protein interactions in human hemoglobin studies by Fourier transform infrared spectroscopy. J Biol Chem 255: 3892–3897

Albrecht AC (1960) On the theory of Raman intensities. J Chem Phys 34: 1476–1484

Antonini E, Brunori M (1971) Hemoglobin and myoglobin in their reaction with ligands. North-Holland, Amsterdam London

Collins DW, Fitchen DB, Lewis A (1973) Resonance Raman scattering from cytochrome c: Frequency dependence of the depolarization ratio. J Chem Phys 59: 5714–5719

Debois A, Lutz M, Banerjee R (1981) Resonance Raman spectra of deoxyhemproteins heme structure in relation to dioxygen bindung. Biochim Biophys Acta 671: 177–183

Eisenberger P, Shulman RG, Brown GS, Ogawa S (1976) Structurefunction relations in hemoglobin as determined by X-ray absorption spectroscopy. Proc Natl Acad Sci USA 73: 491–495

Eisenberger P, Shulman RG, Kincaid BM, Brown GS, Ogawa S (1978) Extended X-ray absorption fine structure determination of iron nitrogen distances in haemoglobin. Nature 274: 30–34

Frauenfelder H, Petsko GA, Tsernoglou D (1979) Temperature-dependent X-ray diffraction as a probe of protein structural dynamics. Nature 280: 559–563

Heidner EJ, Ladner RC, Perutz MF (1976) Structure of horse carbonmonoxyhaemoglobin. J Mol Biol 104: 707–722

Herzfeld J, Stanley HE (1974) A general approach to co-operativity and its application to the oxygen equilibrium of hemoglobin and its effectors. J Mol Biol 82: 231–265

Hopfield JJ (1973) Relation between structure, co-operativity and spectra in a model of hemoglobin action. J Mol Biol 77: 207–222

Hsu MC, Woody RW (1971) The origin of the heme Cotton effects in myoglobin and hemoglobin. J Am Chem Soc 93: 3515–3525

Kilmartin JV, Fogg JH, Perutz MF (1980) Role of C-terminal histidine in the alkaline Bohr effect of human hemoglobin. Biochemistry 19: 3189–3193

LaMar GN, Budd DL, Sick H, Gersonde K (1978) Acid Bohr effects in myoglobin characterized by proton NMR hyperfine shifts and oxygen binding studies. Biochim Biophys Acta 537: 278–283

Lindstrom TR, Ho C (1973) Effects of anions and ligands on the tertiary structure around ligand binding site in human adult hemoglobin. Biochemistry 12: 134–139

Loudon R (1973) The quantum theory of light. Clarendon Press, Oxford

Matthew JB, Hanania GIH, Gurd FRN (1979a) Electrostatic effects in hemoglobin: Hydrogen ion equilibrium in human deoxy- and oxyhemoglobin A. Biochemistry 18: 1919–1928

Matthew JB, Hanania GIH, Gurd FRN (1979b) Electrostatic effects in hemoglobin: Bohr effect and ionic strength dependence of individual groups. Biochemistry 18: 1928–1936

McClain WM (1971) Excited state symmetry assignment through polarized two photon absorption studies of fluid. J Chem Phys 55: 2789–2796

McDonald MI, Noble RWC (1972) The effect on the rates of ligand replacement reactions of human adult and fetal hemoglobus and their subunit. J Biol Chem 247: 4282–4287

Monod J, Wyman J, Changeux JPC (1965) On the nature of allosteric transitions: A plausible model. J Mol Biol 12: 88–118

Nagai K, Kitagawa T, Morimoto H (1980) Quaternary structures and low frequency molecular vibrations of haems of deoxy- and oxyhaemoglobin studied by resonance Raman scattering. J Mol Biol 136: 271–289

Nagai K, LaMar GN, Jue T, Bunn HFC (1982) Proton magnetic resonance investigation of the influence of quarternary structure on iron-histidine bonding in deoxyhaemoglobin. Biochemistry 21: 842–847

el Naggar S, Schweitzer-Stenner R, Dreybrodt W, Mayer A (1984) Determination of the Raman tensor of the haem group in myoglobin by resonance Raman scattering in solution and single crystals. Biophys Struct Mech 10: 257–273

Ondrias MR, Rousseau DL, Shelnutt JA, Simon SR (1982) Quarternary-transformation-induced changes at the heme in deoxyhemoglobins. Biochemistry 21: 3420–3437

Parak F, Kalvius GM (1982) Anwendung des Mößbaereffektes auf Probleme der Biophysik. In: Hoppe F, Lohmann W (Hrsg) Biophysik Springer, Berlin Heidelberg New York, pp 159–183

Perutz MF (1970a) Stereochemistry of cooperative effects in haemoglobin. Nature 228: 726–734

Perutz MF (1970b) The Bohr effect and combination with organic phosphates. Nature 228: 734–739

Peticolas W, Nafie L, Stein P, Fanconi B (1970) Quantum theory of the intensities of molecular vibrational spectra. J Chem Phys 52: 1576–1588

Placzek G (1934) Rayleighstreuung und Ramaneffekt. In: Marx E (Hrsg) Handbuch der Radiologie. Akademische Verlagsgesellschaft, Leipzig

Russu I, Ho NT, Ho C (1982) A proton nuclear magnetic resonance investigation of histidyl residues in human normal adult hemoglobin. Biochemistry 21: 5031–5043

Schweitzer R (1983) Untersuchung von pH-induzierten Symmetrieverzerrungen der prosthetischen Gruppe in Hämoglobin durch resonante Ramanstreuung. Doktorarbeit, Bremen

Schweitzer R, Dreybrodt W, Mayer A, el Naggar S (1982) Influence of the solvent environment on the polarization properties of resonance Raman scattering in haemoglobin. J Raman Spectrosc 13: 139–147

Schweitzer R, Dreybrodt W, el Naggar S (1983) Investigation of pH-induced symmetry distortions of the prosthetic group in haemoglobin by resonance Raman scattering. Jahrestagung der Deutschen Gesellschaft für Biophysik, GSF-Bericht 5/83: 1–29

Schweitzer-Stenner R, Dreybrodt W, el Naggar S (1984) Investigation of pH-induced symmetry distortions of the prosthetic group in deoxyhaemoglobin by resonance Raman scattering. Biophys Struct Mech 10: 241–256

Shelnutt JA (1980) The Raman excitation spectra and absorption spectrum of a metalloporphyrin in an environment of low symmetry. J Chem Phys 72: 3948–3958

Shelnutt JA, Cheung LD, Chang RCC, Nai-Teng Y, Felton RH (1977) Resonance Raman spectra of metalloporyphyrins. Effects of Jahn-Teller instability and nuclear distortions on excitation profiles of Stokes fundamentals. J Chem Phys 66: 3387–3398

Shelnutt JA, Rousseau DL, Friedman JM, Simon SR (1979) Proteinheme interaction in hemoglobin: Evidence from Raman difference spectroscopy. Proc Natl Acad Sci USA 76: 4409–4413

Shelnutt JA, Rousseau DL, Dethmers JK, Margoliash E (1981) Protein influences on porphyrin structure in cytochrome c: Evidence from Raman difference spectroscopy. Biochemistry 20: 6485–6497

Shelnutt JA, Satterlee JD, Erman JE (1983) Raman difference spectroscopy of heme-linked ionization in cytochromic peroxidase. J Biol Chem 258: 2168–2173

Shulman RG, Ogawa S, Mayer A (1982) In: Ho C (ed) The two-state model of hemoglobin, hemoglobin and oxygen binding (Ed. Ho C). Macmillan Press, London, pp 205–209

Soni SK, Kiesow LA (1977) pH-Dependent soret difference spectra of the deoxy and carbonmonoxy forms of human hemoglobin and its derivatives. Biochemistry 16: 1165–1170

Spiro TG, Strekas TC (1974) Resonance Raman spectra of heme proteins. Effects of oxidation and spin state. J Am Chem Soc 96: 338–345

Warshel A, Weiss R (1982) In: Ho C (ed) Strain and electrostatic contributions to cooperativity in hemoglobin, hemoglobin and oxygen binding. Macmillan Press, London, pp 211–216

Wyman J (1966) Allosteric linkage. J Am Chem Soc 89: 2202–2218

El-Yassin DI, Fell DA (1982) Comparison of the applicability of several allosteric models to the pH and 2,3 Bio(phospho) glycerate dependence of oxygen binding by human blood. J Mol Biol 156: 863–889

Zgierski MZ, Pawlikowski M (1982) Depolarization dispersion curves of resonance Raman fundamentals of metalloporphyrins and metallophthalocyanines. Subject to asymmetric perturbations. Chem Phys 65: 335–367